Electronic structure of fullerenelike cages and finite nanotubes of aluminum nitride

Rajendra R. Zope[1,*] and Brett I. Dunlap[2]
[1]*Department of Chemistry, George Washington University, Washington DC, 20052, USA*
[2]*Code 6189, Theoretical Chemistry Section, US Naval Research Laboratory, Washington, DC 20375, USA*
(Received 19 March 2005; revised manuscript received 27 May 2005; published 18 July 2005)

We report a density functional study of alternate fullerenelike cage structures and finite closed, capped single-wall nanotubes of aluminum nitride. The cages and nanotubes studied are modeled as $Al_{24}N_{24}$, $Al_{28}N_{28}$, $Al_{32}N_{32}$, $Al_{36}N_{36}$, $Al_{48}N_{48}$, and $Al_{96}N_{96}$. The structure optimization and calculation of the electronic structure, vertical ionization potential, and the electron affinity are performed at the all-electron level by the analytic Slater-Roothaan method, using a polarized Gaussian basis set of double zeta quality. All structures are energetically stable with binding energy of about 10–11 eV per AlN pair. For the larger $Al_{96}N_{96}$, the fullerenelike cage is energetically less favorable than the *two-shell* cluster that has $Al_{24}N_{24}$ as an inner shell. The vertical ionization potential and the electronic affinity are in the range 6.7–6.9 eV and 1.5–2.0 eV, respectively. The binding energy shows systematic increase with increase in the length of the (4,4) nanotube. The energy band gap, determined using the ΔSCF method, shows that these structures are characterized by a fairly large band gap of about 4–5 eV, which is, however, smaller than the gap for the corresponding boron nitride structures.

DOI: 10.1103/PhysRevB.72.045439 PACS number(s): 73.22.−f, 61.46.+w

I. INTRODUCTION

Aluminum nitride (AlN) belongs to the group III-V family of semiconductors and possesses number of properties such as low thermal expansion (close to that of silicon), high thermal conductivity, resistance to chemicals and gases normally used in semiconductor processing, and good dielectric properties, which make it a potential candidate for technological applications in microelectronics. Unlike another group III-V semiconductor, boron nitride (BN), AlN does not exist in the layered graphitic form, which can be rolled up to form nanotubes. Nevertheless, a few reports of AlN nanotube and nanowire synthesis have appeared in the literature in recent years.[1–5] In the earliest report,[1] the AlN nanotubes (AlN-NT) and nanoparticles were synthesized by dc-arc plasma method and were characterized by the transmission electron microscope (TEM). The nanotubes were measured to be 500–700 nm in length with 30–200 nm diameter, and the nanoparticles had diameters in the 5–200 nm size range. The field emission pattern from tungsten tips coated with AlN tubes was measured and was attributed to the tubes having open ends. Using the same dc-arc plasma method, helical and twisted AlN nanotubes were reported by the same group.[2] The nanotubes were dispersed on graphite substrate and analyzed by scanning tunneling microscopy. The tubes were reported to have an average diameter of 2.2 nm and lateral dimension of about 10 nm. The interatomic distance between two Al—Al or N—N atoms was measured to be 3.2 Å and from *I-V* curves the AlN-NT were argued to be metallic in character.[2] In another study,[3] same group reported synthesis of AlN nanoparticles in the size range 15–18 nm and of nanowires of 500–700 nm in length with diameters in the 30–100 nm size range. In a subsequent report, these nanowires were interpreted to be nanotubes.[4] Synthesis of faceted hexagonal AlN nanotubes has also been reported.[5] These AlN-NT were characterized by TEM and were found to be of a few micrometers in length and 30–80 nm in diameter. Most tubes were found with both ends open. There are also a few reports of theoretical calculations.[6–8] Zhang and Zhang[6] considered two model $Al_{27}N_{27}$ structures, one for an AlN nanowire and one for an AlN nanotube at the Hartree-Fock level using the 3-21G basis set. They noted that AlN bond length in finite AlN-NTs, modeled by the $Al_{27}N_{27}$ tubule, alternates between 1.76 and 1.77 Å and possesses a large energy gap of 10.1 eV between the highest occupied molecular orbital (HOMO) level and the lowest unoccupied molecular orbital (LUMO) level. This rather large gap of 10.1 eV is an artifact of the Hartree-Fock approximation which models exchange effects exactly but ignores correlations effects. Our calculations, on the other hand, calculate the band gap by the so-called ΔSCF where the first ionization potential is subtracted from the first electron affinity. In density functional theory for finite systems, this is known to provide better approximation to the band gap than the significantly underestimated HOMO-LUMO eigenvalue difference. Another theoretical calculation by Zhao and co-workers[7,8] has used density functional theory in the local density approximation (LDA) and generalized gradient approximation (GGA) to study strain energy (energy required to curl up nanotube from graphite like planar sheet) and stability of selected single-walled AlN-NT. These calculations employed a localized numerical orbital basis and psuedopotential for description of ion cores. These authors noted HOMO-LUMO gaps of 3.67 and 3.63 eV for (5, 5) and (9, 0) tubes, respectively. Simulations at elevated temperatures at the level of LDA indicated stability of single walled AlN-NT at room temperature. In the present paper, we report the study of fullerene analog of AlN cages and finite (4, 4) single-walled AlN nanotubes using analytic density functional theory. Unlike AlN-NT, only one study has so far addressed AlN nitride cage structures. The study was performed using density functional theory and indicated possible existence of $Al_{12}N_{12}$, $Al_{24}N_{24}$, and $Al_{60}N_{60}$ on the basis of energetics and vibrational stability.[9] The present study is motivated partly by these works and partly by reports of synthesis of boron nitride (BN) cages.[10–13] Here, we study several fullerene analogs of AlN and selected single-wall AlN nanotubes containing up to about 200 atoms. Some of the cage structures studied in this work have been proposed as candidate structures for boron nitride (BN) cages

synthesized and detected in the mass spectrum.[10–13] Our study, performed at the all electron density functional level, does not preclude the existence of cage structures for the AlN, in agreement with conclusion drawn by Chang and co-workers.[9] The binding energy, the first ionization potential, and electron affinity are calculated. The band gap calculated by the difference of self-consistent solution (ΔSCF) method shows that the cages and tubes of AlN, like their bulk phase, are characterized by a large gap.

II. METHODOLOGY AND COMPUTATIONAL DETAILS

Our calculations are performed using the Slater-Roothaan (SR) method.[14] It uses Gaussian bases to fit the orbitals and effective one-body Kohn-Sham potential of density functional theory.[15] The SR method through robust and variational fitting is analytic and variational in all (orbital and fitting) basis sets.[14] The most general functionals that it can treat so far are certain variants[16] of the $X\alpha$ functional.[17,18] In particular, it can handle different α's on different elements analytically and variationally so that the atomized energies of any cluster can be recovered exactly, and all energies are accurate through first order in any changes to any linear-combination-of-atomic-orbitals LCAO or fit. The *s*-type fitting bases are those scaled from the *s*-part of the orbital basis.[19] A package of basis sets has been optimized[20] for use with DGauss.[21] We use the valence double-ζ orbital basis set DZVP2 and the *pd* part of the (4,3;4,3) (A2) charge density fitting basis. We use the α values of 0.748 222 and 0.767 473 for Al and N, respectively.[22] Using these α values with the above basis sets, exact total energies of Al and N atoms can be obtained. Hence, in the present computational model, the atoms in the cages or tubes will have *exact* atomic energies in the dissociation limit.[23] The accuracy of this method using the exact atomic values of α as judged from the binding energies of Pople's G2 set of molecules lies between that of the local density approximation and that of the generalized gradient approximation.[22] Its main advantage is that it requires no numerical integration and hence within the accuracy of the model gives results that are accurate to machine precision. The optimization is performed using the Broyden-Fletcher-Goldfarb-Shanno (BFGS) algorithm[25–29] with forces on the atoms computed nonrecursively using the 4-*j* generalized Gaunt coefficients.[24]

III. RESULTS AND DISCUSSION

Before we present our results on larger AlN cages, we test the computational model for the simple diatomic AlN molecule, for which experimental values of bond length and dissociation energy are available. A number of theoretical calculations at different levels of sophistication have also been performed on this molecule.[31–35] The comparison of these with the numbers obtained in present model is given in Table I, where the present values are found to be in good agreement with the experimental values. All theoretical values of dissociation energy are within the rather large experimental error bar. Predicted dissociation energy in the present model lies between the *ab initio coupled cluster* (CCSD) and *multi reference configuration interaction* MRCI numbers on the one hand and the Becke-Perdew86 (BP86) or Becke-Perdew-Wang91 (BPW91) density functional models on the other. Use of larger 6-311G** orbital basis and the Turbomole fitting basis used in our earlier work[22,36] does not change the results. Bond length is practically identical and the binding energy decreases by 0.2 eV. The basis set effect is largely cancelled by adjusting α to get exact the atomic energies. Thus, we expect the present model to provide a reliable description of AlN cages and nanotubes studied in this work.

TABLE I. The bond length and dissociation energy of $^3\Pi$ AlN molecule obtained by present analytic Slater-Roothan method in comparison with those obtained from some selected computational models and experiment. The present value of dissociation energy does not contain zero point energy.

Model	Reference	R_e (Å)	D_0 (eV)
Experiment	30	1.79	2.86±0.39
CCSD(T)/WMR	32	1.79	2.45
MRCI	31	1.83	2.42
MRCI	33	1.81	2.20
BP86/6-31G*	34	1.81	2.87
BPW91/6-31G**	35	1.80	2.76
Present		1.81	2.71

The optimized $Al_{24}N_{24}$ clusters of octahedral, S_4, and S_8 symmetry are shown in Fig. 1. The octahedral cage consists of six octagons, eight squares, and eight hexagons. It is a round cage with two symmetry inequivalent atoms. This round cage has been studied as a candidate for cages made up of carbon,[37] silicon hydrides,[38] boron oxides,[38] aluminum hydrides,[38] etc. It has also been proposed as the structure of the $B_{24}N_{24}$ peak, found in abundance in a recent experimental time-of-flight, mass spectrometric study.[11] The optimized coordinates of the $Al_{24}N_{24}$ cage for two inequivalent atoms in Å are (0.868, 2.101, 3.326) for Al and (3.48, 2.13, 0.916) for N, respectively. Positions of other atoms can be determined from the symmetry group operations of an octahedral point group with symmetry axes along the coordinate axes. The cage has a radius of 4.11 Å, about 27% larger than that of the octahedral $B_{24}N_{24}$ cage.[39] The Al atoms are on the sphere of 4.03 Å radius, while the N atoms lie on the sphere of 4.18 Å. These differences in radii of Al and N skeletons are of the same magnitude to those found for the B and N radii in the $B_{24}N_{24}$ cage. In contrast, the S_4 cage, also shown in Fig. 1, satisfies the isolated six square hypothesis[40] and does not contain any octagon. The isolated square hypothesis is similar to the better-known isolated pentagon rule for carbon fullerenes. The exact AlN analog of carbon fullerenes do not exist. Fullerenes do not permit full alternation of aluminum and nitrogen atoms due to the presence of pentagonal rings. Even-numbered rings are necessary in alternate cages. Using Eüler's theorem, it can be shown that alternate AlN cages can be made closed using exactly six squares (four atom rings). The S_4 structures is such a cage containing 20 hexagons and six squares. It is proposed as a fullerenelike analog of an alternate boron nitride fullerene.

The S_8 cage contains two octagons, eight squares, and 12 hexagons. It is indistinguishable from the *O* cage when

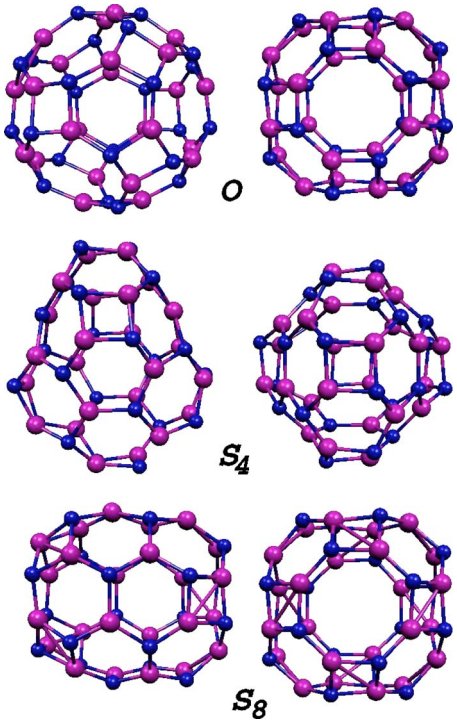

FIG. 1. (Color online) Two different views of optimized octahedral O, S_4, and S_8 $Al_{24}N_{24}$ cages.

viewed along the fourfold axis passing through the center of the octagon. It is basically a very short closed capped (4, 4) armchair aluminum nitride nanotube. As it is practiced in the literature we use the term nanotube for cylindrical cage structures. Incidentally, the caps of (4, 4) armchair AlN NT are the hemispherical halves of round octahedral O cage.[39] boron nitride nanotube. For boron nitride, the S_8 and S_4 cages are energetically favored over the O cage, although the energy differences were quite small.[39,46] In the present $Al_{24}N_{24}$ case, a similar trend is observed and the energy differences are further diminished. The S_4 and S_8 cages are energetically nearly degenerate with the O cage being higher by 0.1 eV.

The S_8 $Al_{24}N_{24}$ cage can be extended along the fourfold axis by inserting a ring of alternate AlN pairs to obtain $Al_{28}N_{28}$ nanotubes with C_{4h} symmetry (Fig. 2). The C_{4h} $Al_{28}N_{28}$ tube can also be generated from the O $Al_{24}N_{24}$ cage by cutting former into two halves, orienting them along the C_4 axis, and then inserting a ring of eight alternate AlN atoms, followed by a rotation of one half by 45°. Likewise, the C_{4h} $Al_{28}N_{28}$ tube can be extended by adding one and five rings of alternate AlN atoms to obtain $Al_{32}N_{32}$ and $Al_{48}N_{48}$ nanotubes, respectively. Both nanotubes have S_8 symmetry. The addition of successive alternate rings will lead to the more familiar infinite (4,4) AlN nanotube. The optimized structures of the capped nanotubes thus derived are shown in Fig. 3. The tubes have diameter of 6.68 Å. The largest tube $Al_{48}N_{48}$ has length of 16.5 Å. The AlN bond lengths in tubes in general vary from 1.74 to 1.80 Å. The AlN bond that shares hexagonal and octagonal rings is the shortest (1.74 Å) while the largest one (1.80 Å) is shared by octagonal and square rings. The inner hexagonal rings have AlN bond distances in the range 1.76–1.79 Å.

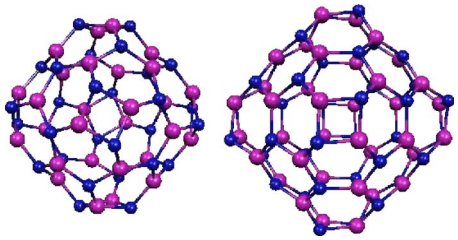

FIG. 2. (Color online) Favorable T $Al_{28}N_{28}$ and T_d $Al_{36}N_{36}$ cages containing six squares.

The $Al_{28}N_{28}$ cage of T symmetry and the tetrahedral $Al_{36}N_{36}$ cage (Fig. 2) are another two cages that satisfy the isolated six square hypothesis, and thus prior to the experimental boron nitride work[11] were considered most favorable. The former contains 24 hexagons while the later has 32 hexagons. The boron nitride counterparts of both these structures have been proposed as candidate structures for abundant boron nitride clusters detected in mass spectrum. The $Al_{28}N_{28}$ cage of T symmetry is energetically more favorable than the C_{4h} $Al_{28}N_{28}$ nanotube. The former has six fourfold rings that are isolated by hexagonal rings while the latter has more defects, eight squares and two octagons. The extra defects in the C_{4h} make it energetically less favorable. Our calculations show that the AlN bond distances in the T_d cage are largest (1.80 Å) for the bonds that belong to the square ring. The bonds between a square and hexagon are 1.76 Å in length, and those between hexagonal rings have length of 1.79 Å.

The $Al_{96}N_{96}$ cluster is a larger cage that preserves the symmetry of the $Al_{24}N_{24}$ by surrounding all square and oc-

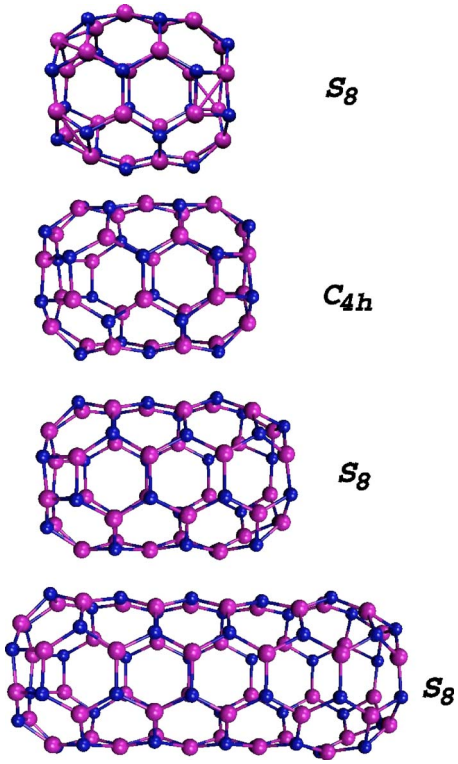

FIG. 3. (Color online) Finite AlN nanotubes: $Al_{24}N_{24}$, $Al_{28}N_{28}$, $Al_{32}N_{32}$, and $Al_{48}N_{48}$.

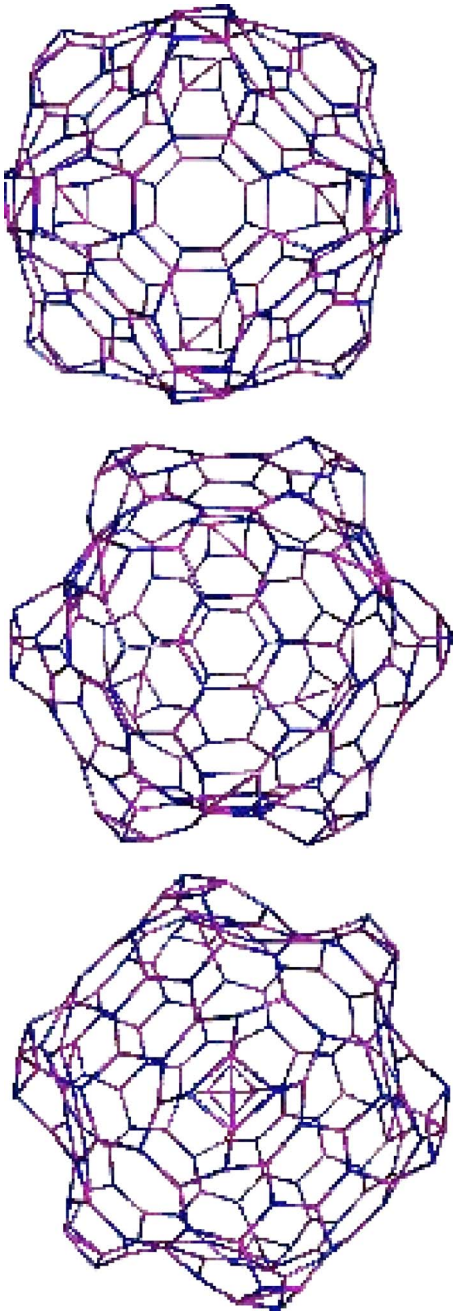

FIG. 4. (Color online) Octahedral $Al_{96}N_{96}$-I cage as seen from the fourfold (top), threefold (middle), and twofold (bottom) axes, respectively.

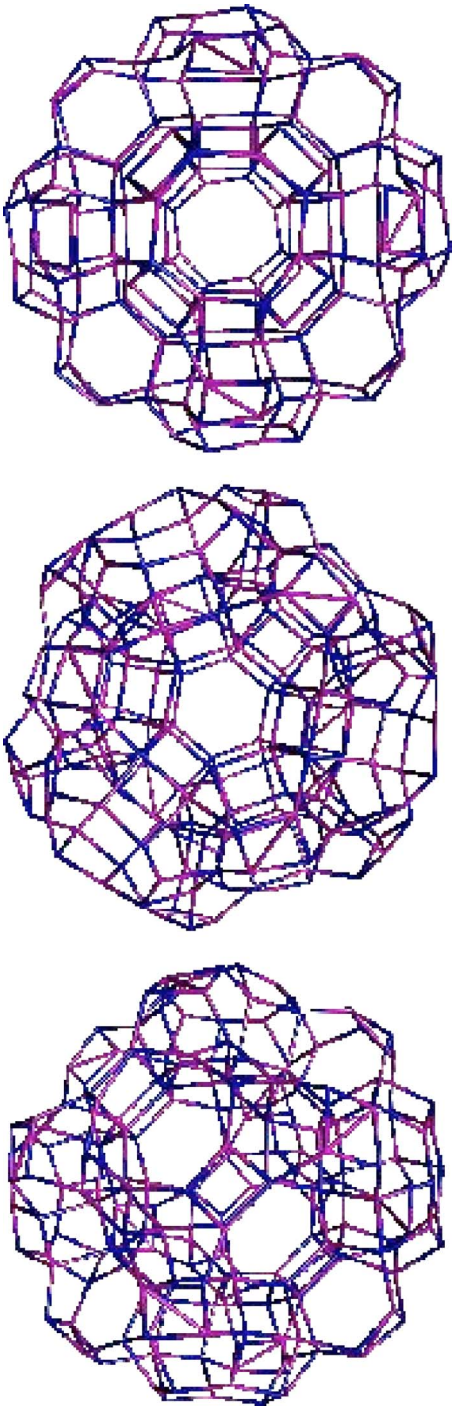

FIG. 5. (Color online) Octahedral $Al_{96}N_{96}$-II cage as seen from the fourfold (top), threefold (middle), and twofold (bottom) axes, respectively.

tagonal defects by rings of hexagons like leapfrogging in the fullerenes,[41] which also leads to a cluster four times as big. Leapfrog fullerenes necessarily have closed electronic shells. All III–V fullerenelike clusters have closed shells due to large HOMO-LUMO gaps. The $Al_{96}N_{96}$ cage contains 18 defects: 12 squares and six octagons. The optimization of $Al_{96}N_{96}$, starting from the ionic configuration of the $B_{96}N_{96}$ cage scaled by roughly the ratio of AlN and BN average bond distances, results in the fullerenelike $Al_{96}N_{96}$-I cage as shown in Fig. 4. It is evident from the figure that squares stick out. The cage has an average radius of 7.5 Å and squares protrude out by roughly 1 Å from the average radius.

On the other hand, if the optimization of $Al_{96}N_{96}$ is started from the unscaled $B_{96}N_{96}$ cage, then one obtains a very different *O* structure. The resultant structure, called two-shell $Al_{96}N_{96}$-II cage hereafter, is shown in Fig. 5. It is very different from the $Al_{96}N_{96}$-I cage in Fig. 4 and is basically surface growth on the octahedral $Al_{24}N_{24}$ cage. The $Al_{24}N_{24}$ core of this structure is evident in Fig. 5. The atoms on the surface of inner core have fourfold coordination. The two-shell cage is lower in energy by 0.66 Hartree than the

TABLE II. The electronic structure and symmetry of HOMO and LUMO of the AlN cages and nanotubes.

System		Electronic structure	HOMO	LUMO
$Al_{24}N_{24}$	O	$10a_1\ 10a_2\ 30t_1\ 30t_2\ 20e$	e	a_1
$Al_{24}N_{24}$	S_4	$60a\ 60b\ 120e$	e	a
$Al_{24}N_{24}$	S_8	$30a\ 30b\ 60e_1\ 60e_2\ 60e_3$	a	a
$Al_{28}N_{28}$	C_{4h}	$38a_g\ 32a_u\ 38b_g\ 32b_u\ 64e_g\ 76e_u$	a_u	a_g
$Al_{28}N_{28}$	T	$26a\ 44e\ 70t$	t	a
$Al_{32}N_{32}$	S_8	$40a\ 40b\ 80e_1\ 80e_2\ 80e_3$	b	a
$Al_{36}N_{36}$	T_d	$24a_1\ 6a_2\ 30e\ 36t_1\ 54t_2$	t_2	a_1
$Al_{48}N_{48}$	S_8	$60a\ 60b\ 120e_1\ 120e_2\ 120e_3$	a	a
$Al_{96}N_{96}$-I	O	$40a_1\ 40a_2\ 80e\ 120t_1\ 120t_2$	a_2	a_1
$Al_{96}N_{96}$-II	O	$40a_1\ 40a_2\ 80e\ 120t_1\ 120t_2$	a_2	a_1

fullerenelike cage despite having many more defects than the fullerenelike $Al_{96}N_{96}$-I cage. From this result it appears that larger spherical clusters or quantum dots of AlN would prefer solidlike cages rather than hollow fullerenelike cages. On the other hand, earlier studies have found a larger $Al_{60}N_{60}$ cage to be energetically and vibrationally stable.[9] It would therefore be interesting to investigate relative stability of larger clusters containing fullerenelike and solidlike spherical quantum dots. We also examined the two-shell cage as a candidate structure of $B_{96}N_{96}$. Our calculation indicates that the cluster is not stable and fragments upon optimization.

The electronic structures of AlN cages are given in Table II while the binding energies per AlN pair, the HOMO-LUMO gaps, the ionization potential, and the electron affinity of these cages are given in Table III. The ionization potential (electron affinity) is calculated from the difference in the self-consistent solutions of neutral AlN cage and its cation(anion). All structures are energetically stable with binding energies of order of 10–11 eV per AlN pair. It is well known that the HOMO-LUMO gaps obtained from the density functional models including the present one underestimate true band gap.[42] The so-called ΔSCF provides good approximation for the ionization potential and the electron affinity of the system.[43] We determine the band gap as a difference of ionization potential and electron affinity computed by the ΔSCF method. The time-dependent density functional theory (TDDFT) or the *GW* approximation provide corrections to the HOMO-LUMO gaps and are more suitable for calculations of the band gaps. We have not yet implemented these techniques. However, the present methodology of using fitting basis sets can also make TDDFT calculations efficient.[44] The ΔSCF calculated gaps are given in Table III. In the case of $Al_{24}N_{24}$, although the O cage is energetically less favorable, its HOMO-LUMO gap and ΔSCF gap are larger than those of the S_4 and S_8 cages. Amongst the AlN cages that have only six isolated squares, the binding energy systematically increases for S_8 $Al_{24}N_{24}$, T $Al_{28}N_{28}$, and $Al_{36}N_{36}$ cages. This trend is similar to that observed in the case of boron nitride cages[39] and carbon fullerenes.[45] The squares stick out too far in the $M_{96}N_{96}$ (M=B, Al) cage for that cage to be favored and its hemisphere to be an extremely favorable cap of the (8,8) nanotubes. Both the $Al_{96}N_{96}$ cages have smaller binding energy than the $Al_{48}N_{48}$ nanotube, perhaps due to larger number of defects (octagonal and fourfold rings). The O $Al_{24}N_{24}$ and $Al_{60}N_{60}$ cages were also studied by Change *et al.*[9] They find that the former has binding energy of 4.72 eV atom^{-1} while the latter has binding energy of 4.76 eV atom^{-1}. The increase in the binding energy from octahedral $Al_{24}N_{24}$ cage to $Al_{60}N_{60}$ cage is 0.05 eV atom^{-1}. Our calculations show binding energy gain of 0.4 eV atom^{-1} with size increase from octahedral $Al_{24}N_{24}$ to octahedral $Al_{96}N_{96}$. It is therefore likely that the octahedral cages studied in this work are more stable than the icosahedral $Al_{60}N_{60}$ cage. In comparison with their boron nitride counterparts[39,46,47] the AlN cages are energetically less stable and have lower ionization potentials and smaller band gaps. This feature is similar to the bulk phase of these materials. The band gap of solid AlN is smaller than that of BN solids.

TABLE III. The calculated values of binding energy per AlN pair (BE), the energy gap between the highest occupied molecular orbital and the lowest unoccupied molecular orbital, the vertical ionization potential (VIP), the electron affinity (VEA), and the energy gap obtained from the ΔSCF calculation for the optimized AlN cages. These calculations are spin-polarized. All energies are in eV.

	Symmetry	BE	GAP	VIP	VEA	ΔSCF
$Al_{24}N_{24}$	O	10.24	2.97	7.05	1.46	5.59
$Al_{24}N_{24}$	S_4	10.34	2.47	6.84	1.72	5.12
$Al_{24}N_{24}$	S_8	10.34	2.63	6.79	1.58	5.21
$Al_{28}N_{28}$	C_{4h}	10.42	2.74	6.81	1.59	5.22
$Al_{28}N_{28}$	T	10.45	2.67	6.84	1.69	5.15
$Al_{32}N_{32}$	S_8	10.49	2.79	6.77	1.61	5.16
$Al_{36}N_{36}$	T_d	10.54	2.70	6.73	1.76	4.95
$Al_{48}N_{48}$	S_d	11.09	2.81	6.56	1.76	4.8
$Al_{96}N_{96}$-I	O	10.56	2.63	6.22	2.04	4.12
$Al_{96}N_{96}$-II	O	10.75	1.81	6.03	2.53	3.50

To summarize, fullerenelike cage structures and finite (4,4) nanotubes are studied by the density functional calculations using polarized Gaussian basis sets of double zeta quality. The binding energy, electron affinity, ionization potential, the HOMO-LUMO gap, and the ΔSCF gap are calculated for the optimized AlN cages. Calculations show that all AlN cages are energetically stable, with band gap of order of 5 eV. For the larger $Al_{96}N_{96}$ cluster, the *two-shell* cage with an interior $Al_{24}N_{24}$ O cage is energetically favorable over the fullerene-like cage. The binding energies and band gaps are smaller than their BN counterparts. We hope that the present study will aid the experimental search for the AlN cages.

The Office of Naval Research, directly and through the Naval Research Laboratory, and the Department of Defense's High Performance Computing Modernization Program, through the Common High Performance Computing Software Support Initiative Project MBD-5, supported this work.

*Present mailing address: Theoretical Chemistry Section, Naval Research Laboratory, Washington DC 20375, USA.
[1] V. N. Tondare, C. Balasubramanian, S. V. Shende, D. S. Joag, V. P. Godbole, and S. V. Bhoraskar, Appl. Phys. Lett. **80**, 4813 (2002).
[2] C. Balasubramanian, S. Bellucci, P. Castrucci, M. De Crescenzi, and S. V. Bhoraskar, Chem. Phys. Lett. **383**, 188 (2004).
[3] C. Balasubramanian, V. P. Godbole, V. K. Rohatgi, A. K. Das, and S. V. Bhoraskar, Nanotechnology **15**, 370 (2004).
[4] V. Tondare, Nanotechnology **15**, 1388 (2004).
[5] Q. Wu, Z. Hu, X. Wang, Y. Lu, X. Chen, H. Xu, and Y. Chen, J. Am. Chem. Soc. **125**, 10176 (2003).
[6] D. Zhang and R. Q. Zhang, Chem. Phys. Lett. **371**, 426 (2003).
[7] M. Zhao, Y. Xia, Z. Tan, X. Liu, F. Li, B. Huang, Y. Ji, and L. Mei, Chem. Phys. Lett. **389**, 160 (2004).
[8] M. Zhao, Y. Xia, D. Zhang, and L. Mei, Phys. Rev. B **68**, 235415 (2005).
[9] C. Chang, A. B. C. Patzer, E. Sedlmayr, T. Steinke, and D. Sülze, Chem. Phys. Lett. **350**, 399 (2001).
[10] T. Oku, T. Hirano, M. Kuno, T. Kusunose, K. Nihara, and K. Suanuma, Mater. Sci. Eng., B **B74**, 206 (2000).
[11] T. Oku, A. Nishiwaki, I. Narita, and M. Gonda, Chem. Phys. Lett. **380**, 620 (2003).
[12] O. Stephan, Y. Bando, A. Loiseau, F. Willamie, N. Shramchenko, T. Tamiya, and T. Sato, Appl. Phys. A: Mater. Sci. Process. **67**, 107 (1998).
[13] D. Goldberg, Y. Bando, O. Ste'pahan, and K. Kurashima, Appl. Phys. Lett. **73**, 2441 (1998).
[14] B. I. Dunlap, J. Phys. Chem. **107**, 10082 (2003).
[15] W. Kohn and L. J. Sham, Phys. Rev. **140**, A1133 (1965).
[16] E. C. Vauthier, A. Cossé-Barbi, M. Blain, and S. Fliszár, J. Mol. Struct.: THEOCHEM **492**, 113 (1999).
[17] R. P. Messmer, S. K. Knudson, K. H. Johnson, J. B. Diamond, and C. Y. Yang, Phys. Rev. B **13**, 1396 (1976).
[18] Y. Takai and K. H. Johnson, Chem. Phys. Lett. **189**, 518 (1992).
[19] B. I. Dunlap, J. W. D. Connolly, and J. R. Sabin, J. Chem. Phys. **71**, 3396 (1979); **71**, 4993 (1979).
[20] N. Godbout, D. R. Salahub, J. Andzelm, and E. Wimmer, Can. J. Chem. **70**, 560 (1992).
[21] J. Andzelm and E. Wimmer, J. Phys. B **172**, 307 (1991); J. Chem. Phys. **96**, 1280 (1992).
[22] R. R. Zope and B. I. Dunlap, cond-mat/0410129 (http://xxx.lanl.gov).
[23] K. H. Johnson, Annu. Rev. Phys. Chem. **26**, 39 (1975).
[24] B. I. Dunlap, Phys. Rev. A **66**, 032502 (2002).
[25] G. Broyden, J. Inst. Math. Appl. **6**, 222 (1970).
[26] R. Fletcher, Comput. J. **13**, 317 (1970).
[27] D. Goldfarb, Math. Comput. **24**, 23 (1970).
[28] D. F. Shanno, Math. Comput. **24**, 647 (1970).
[29] W. H. Press, B. P. Flannery, S. A. Teukolsky, and W. T. Vetterling, *Numerical Recipes The Art of Scientific Computing* (Cambridge U. P., Cambridge, England, 1986), p. 309.
[30] M. W. Chase, J. Phys. Chem. Ref. Data Monogr., *NIST-JANAF Thermochemical Tablles*, 4th ed. (ACS, AIP, NSRDS, Gaithesburg, 1998).
[31] M. Pelissier and J. P. Malrieu, J. Mol. Spectrosc. **77**, 322 (1979).
[32] G. L. Gustev, P. Jena, and R. J. Bartlett, J. Chem. Phys. **110**, 2928 (1999).
[33] S. R. Langhoff, C. W. Bauschlicher, and L. G. M. Petterson, J. Chem. Phys. **89**, 7354 (1988).
[34] C. Chang, A. B. C. Patzer, E. Sedlmayr, T. Steinke, and D. Sülze, Chem. Phys. **271**, 283 (2001).
[35] A. Costales and R. Pandey, J. Phys. Chem. A **107**, 191 (2003).
[36] R. R. Zope and B. I. Dunlap, Phys. Rev. B **71**, 193104 (2005).
[37] B. I. Dunlap and R. Taylor, J. Phys. Chem. **98**, 11018 (1994).
[38] R. A. LaViolette and M. T. Benson, J. Chem. Phys. **112**, 9269 (2000).
[39] R. R. Zope and B. I. Dunlap, Chem. Phys. Lett. **386**, 403 (2004).
[40] M.-L. Sun, Z. Slanina, and S.-L. Lee, Chem. Phys. Lett. **233**, 279 (1995).
[41] P. W. Fowler and D. B. Redmond, Theor. Chim. Acta **83**, 367 (1992).
[42] L. J. Sham and M. Schlüter, Phys. Rev. B **32**, 003883 (1985); R. W. Godby, M. Schlüter, and L. J. Sham, *ibid.* **37**, 10159 (1988).
[43] O. A. Vydrov and G. E. Scuseria, J. Chem. Phys. **122**, 184107 (2005) and references therein.
[44] H. H. Heinze, A. Görling, and N. Rösch, J. Chem. Phys. **113**, 2088 (2005).
[45] B. I. Dunlap, D. W. Brenner, J. W. Mintmire, R. C. Mowery, and C. T. White, J. Phys. Chem. **95**, 8737 (1991).
[46] R. R. Zope, T. Baruah, M. R. Pederson, and B. I. Dunlap, Chem. Phys. Lett. **393**, 300 (2004).
[47] R. R. Zope, T. Baruah, M. R. Pederson, and B. I. Dunlap, Phys. Rev. A **71**, 025201 (2005).